

Annihilation of topological solitons in magnetism: How domain walls collide and vanish to burst spin waves and pump electronic spin current of broadband frequencies

Marko D. Petrović,^{1,2} Petr Plecháč,¹ and Branislav K. Nikolić^{2,*}

¹*Department of Mathematical Sciences, University of Delaware, Newark, DE 19716, USA*

²*Department of Physics and Astronomy, University of Delaware, Newark, DE 19716, USA*

We not only reproduce computationally the burst of spin waves (SWs) of very short wavelengths observed in recent experiments [S. Woo *et al.*, Nat. Phys. **13**, 448 (2017)] where magnetic field drives annihilation of two domain walls (DWs) within a ferromagnetic nanowire, but furthermore we predict that this will be accompanied by a peculiar pumping of electronic spin currents in the absence of any bias voltage. Prior to the instant of annihilation, their power spectrum is *broadband* with finite width around a mean frequency, collapsing to the usual narrow peak around a single frequency after annihilation. The pumping stems from time-dependent fields introduced into the quantum Hamiltonian of conduction electrons by the classical dynamics of localized magnetic moments comprising the domains. The pumped currents carry spin-polarized electrons which, in turn, exert spin-transfer torque on localized magnetic moments, so that the self-consistent nonequilibrium state of the whole system *cannot* be captured by standard classical micromagnetic simulations where conduction electrons are completely absent. Instead, we use recently developed multiscale framework, combining time-dependent electronic nonequilibrium Green functions with the Landau-Lifshitz-Gilbert (LLG) equation, to simulate coupled dynamics of magnetic moments and conduction electrons. The pumped currents inside the annihilation region effectively generate time-retarded damping in the LLG equation which can dramatically affect the SW spectrum. They will also flow out of the annihilation region, where they can be converted into rapidly changing in time charge currents via the inverse spin Hall effect as a potential source of broadband electromagnetic radiation.

The control of the domain wall (DW) motion [1, 2] within magnetic nanowires by magnetic field or current pulses is both a fundamental problem for nonequilibrium quantum many-body physics and a building block of envisaged applications in digital memories [3], logic [4] and artificial neural networks [5]. Since in such devices DWs will be closely packed, understanding interaction between them is a problem of great interest [6]. For example, head-to-head or tail-to-tail DWs—illustrated as the left (L) or right (R) noncollinear texture of localized magnetic moments, respectively, in Fig. 1—behave as free magnetic monopoles carrying topological charge [7]. The topological charge (or the winding number) $Q \equiv -\frac{1}{\pi} \int dx \partial_x \phi$, associated with winding of localized magnetic moments as they interpolate between two uniform degenerate ground states with $\phi = 0$ or $\phi = \pi$, is opposite for adjacent DWs, such as $Q_L = -1$ and $Q_R = +1$ for DWs in Fig. 1. Thus, long-range attractive interaction between DWs can lead to their *annihilation*, resulting in the ground state without any DWs [8–11] (short-range repulsive interaction can also suppress annihilation [6]), while conserving the total topological charge, $Q_L + Q_R = 0$. The nonequilibrium dynamics generated by annihilation of topological solitons, such as DWs or other nonlinear excitations protected by their nontrivial topology, is also of great interest in a surprisingly wide range of fields, ranging from cosmology [12] and quantum field [13] and string [14] theory to liquid crystals [17] and Bose-Einstein condensates [15, 16].

The recent experiments [18] have monitored annihilation of two DWs within a metallic magnetic nanowire by observing intense burst of spin waves (SWs) at the

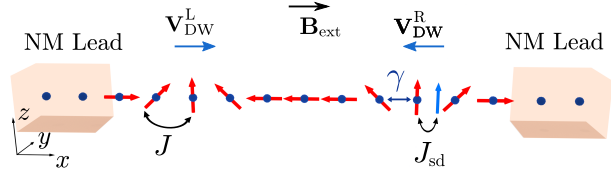


FIG. 1. Schematic view of a metallic magnetic nanowire modeled as a 1D tight-binding chain whose sites also host classical localized magnetic moments (red arrows) interacting with spins (blue arrow) of conduction electrons. The nanowire is attached to two NM leads terminating into the macroscopic reservoirs kept at the same chemical potential. The two DWs within the nanowire carry opposite topological charge [7], $Q_L = -1$ for the left one and $Q_R = +1$ for the right one. The DWs are colliding with the opposite velocities \mathbf{V}_{DW}^L and \mathbf{V}_{DW}^R , and eventually annihilating, upon application of an external magnetic field \mathbf{B}_{ext} parallel to the nanowire, thereby mimicking the setup of the experiments in Ref. [18].

moment of annihilation. Thus generated large-amplitude SWs are dominated by exchange, rather than dipolar, interaction between magnetic moments and are, therefore, of short wavelength. The SWs of ~ 10 nm wavelength are crucial for scalability of magnonics-based technologies [19, 20], like signal transmission or memory-in-logic and logic-in-memory low-power digital computing architectures. However, they are difficult to excite by other means due to the requirement for high external magnetic fields [21, 22].

The computational simulations of DW annihilation [8, 9, 18], together with theoretical analysis of generic features of such a phenomenon [10], have been based ex-

clusively on classical micromagnetics where one solves a system of coupled Landau-Lifshitz-Gilbert (LLG) equations [23] for the dynamics of localized magnetic moments viewed as classical vectors of the fixed length, as justified in the limit of large localized spins $S_i \rightarrow \infty$, $\hbar \rightarrow 0$ (but $S_i \times \hbar \rightarrow 1$) and in the absence of entanglement [24]. On the other hand, the dynamics of localized magnetic moments comprising two DWs also generates time-dependent fields experienced by the surrounding conduction electrons within the magnetic nanowire. This can lead to pumping of electronic spin currents [25, 26] (as well as pumping of charge currents if the left-right symmetry of the device is broken [27–29]) in the absence of any externally applied bias voltage. The spin-polarized electrons carried by such currents will exert spin-transfer torque (STT) on the localized magnetic moments. This can effectively introduce time-retarded damping with a memory kernel [30] into the LLG equation due to the fact that the electron spin can never follow instantaneously a change in the orientation of the localized magnetic moments [31]. Such complicated self-consistent problem cannot be captured by conventional classical micromagnetics [23] where quantum dynamics of electrons is not modeled at all, while torque and damping terms [32, 33] in the LLG equation are introduced phenomenologically with their magnitude specified by the parameters which *do not vary* in time or space [34]. Attempts to introduce phenomenologically time-retarded damping and, thereby, construct an extended LLG equation leads to many possible forms [35, 36] some of which can substantially affect the SW spectrum [35].

In this Letter, we analyze DW annihilation by employing recently developed [26, 30, 37] multiscale *time-dependent-quantum-transport/classical-micromagnetics* framework which combines time-dependent nonequilibrium Green function (TDNEGF) [38, 39] description of quantum dynamics of electrons with the LLG equation description of classical dynamics of localized magnetic moments. Such TDNEGF+LLG framework is microscopic and nonperturbative, once the Hamiltonians of quantum subsystem of conduction electrons and classical subsystem of localized magnetic moments are specified. We apply it to a setup depicted in Fig. 1 where two DWs reside at time $t = 0$ within a one-dimensional (1D) magnetic nanowire attached to two normal metal (NM) leads, terminating into the macroscopic reservoirs *without* any bias voltage being applied between them.

The classical Hamiltonian for localized magnetic moments, described by unit vectors $\mathbf{M}_i(t)$ at each site i of 1D lattice, is chosen as

$$\mathcal{H} = -J \sum_{\langle i,j \rangle} \mathbf{M}_i \cdot \mathbf{M}_j - J_{sd} \sum_i \langle \hat{\mathbf{S}} \rangle_i^{\text{neq}} \cdot \mathbf{M}_i - K \sum_i (M_i^x)^2 + D \sum_i (M_i^y)^2 - \mu_B \sum_i \mathbf{M}_i \cdot \mathbf{B}_{\text{ext}}, \quad (1)$$

where $J = 0.1$ eV is the Heisenberg exchange cou-

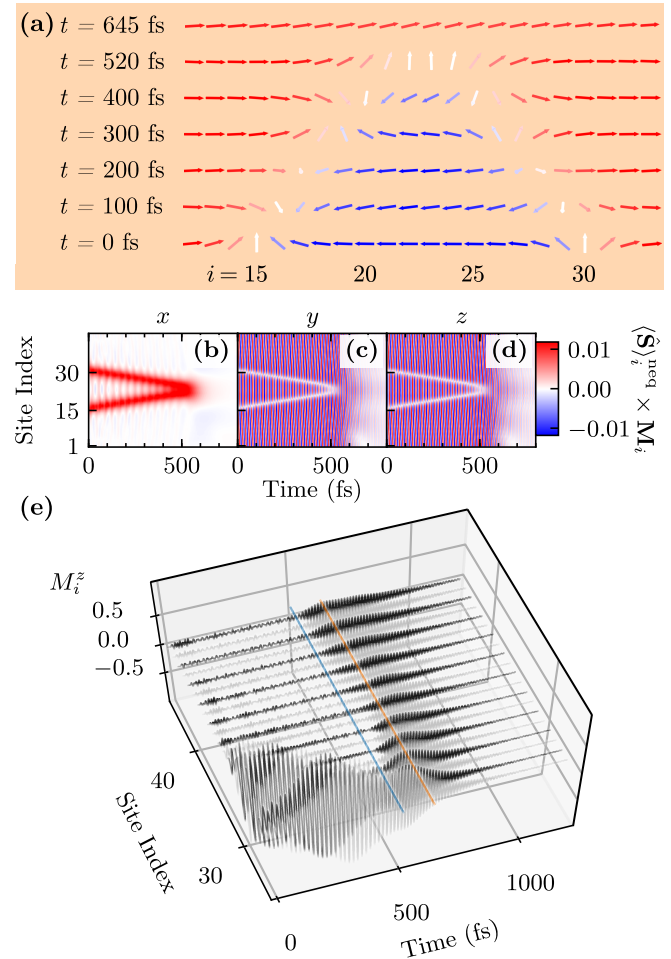


FIG. 2. TDNEGF+LLG computed: (a) sequence of snapshots of two DWs in the course of their collision and annihilation driven by the applied magnetic field \mathbf{B}_{ext} in the setup of Fig. 1; (b)–(d) spatio-temporal profiles of STT $\propto \langle \hat{\mathbf{S}} \rangle_i^{\text{neq}}(t) \times \mathbf{M}_i(t)$ on localized magnetic moments $\mathbf{M}_i(t)$; and (e) spatio-temporal profiles of the z -component of localized magnetic moments where blue and orange line mark times $t = 520$ fs (when two DWs vanish) and $t = 645$ fs (when all localized magnetic moments become nearly parallel to the x -axis) from panel (a). The intrinsic Gilbert damping parameter is $\lambda = 0.01$ and the Fermi energy is $E_F = 0$ eV. A movie animating panels (a) and (e) is provided in the SM [43].

pling between neighboring magnetic moments and $J_{sd} = 0.1$ eV is the *s-d* exchange coupling between the localized magnetic moments and the nonequilibrium electronic spin density

$$\langle \hat{\mathbf{S}} \rangle_i^{\text{neq}}(t) = \frac{\hbar}{2} \text{Tr}_{\text{spin}} \{ [\rho_{\text{neq}}(t) - \rho_{\text{eq}}] \hat{\sigma} \}. \quad (2)$$

This quantity is obtained [26, 40] as the quantum-statistical expectation value of the spin- $\frac{1}{2}$ operator using the time-dependent nonequilibrium density matrix, $\rho_{\text{neq}}(t)$, and the grand canonical density matrix in equilibrium, ρ_{eq} . Here $\hat{\sigma} = (\hat{\sigma}_x, \hat{\sigma}_y, \hat{\sigma}_z)$ is the vector of the

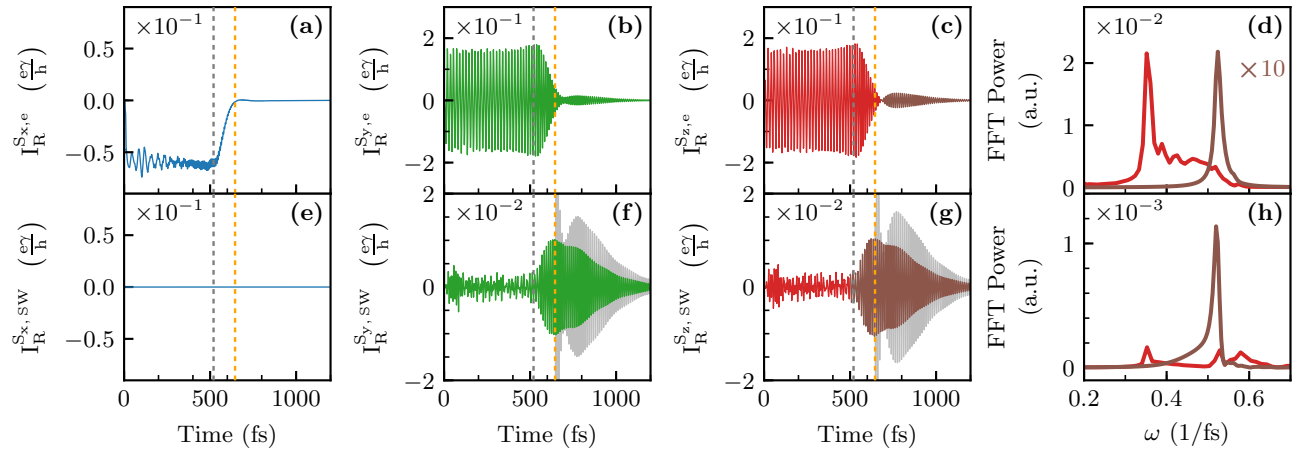


FIG. 3. TDNEGF+LLG computed time-dependence of: (a)–(c) electronic spin currents pumped into the right NM lead during DW collision and annihilation; (e)–(g) SW-generated contribution to spin currents in panels (a)–(c), respectively, after spin current carried by the SW from Fig. 2(e) is stopped at the magnetic-nanowire/nonmagnetic-NM-lead interface and converted (as observed experimentally [18, 46]) into electronic spin current in the right NM lead. Vertical dashed lines mark times $t = 520$ fs and $t = 645$ fs whose snapshots of localized magnetic moments are given in Fig. 2(a). Gray curves in panels (f) and (g) are the same as the signal in panels (b) and (c) for times $t \geq 645$ fs, respectively, and are displayed for an easy comparison. Panels (d) and (h) plot frequency power spectra obtained from FFT of signals in panels (c) and (g), respectively, before (red curve) and after (brown curves) annihilation. The intrinsic Gilbert damping parameter $\lambda = 0.01$ and the Fermi energy is $E_F = 0$ eV.

Pauli matrices and trace is performed in the spin space. The magnetic anisotropy along the x -axis is specified by $K = 0.05$ eV, and the demagnetizing field along the y -axis is $D = 0.007$ eV. The last term in Eq. (1) is Zeeman energy (μ_B is the Bohr magneton) describing the interaction of localized magnetic moments with an external magnetic field $|\mathbf{B}_{\text{ext}}| = 2000$ T which we introduce parallel to the nanowire in Fig. 1 to drive the DW dynamics, as employed in the experiments of Ref. [18]. Taking into account computational complexity of TDNEGF calculations [39], such unrealistically large magnetic field is chosen for computational convenience to allow us to complete DW annihilation on \sim ps time scale (in the experiments [18] DW annihilation occurs within ~ 2 ns). The classical dynamics of $\mathbf{M}_i(t)$ is obtained by solving a system of coupled LLG equations

$$\frac{\partial \mathbf{M}_i}{\partial t} = -\frac{g}{1+\lambda^2} [\mathbf{M}_i \times \mathbf{B}_{\text{eff}}^i + \lambda \mathbf{M}_i \times (\mathbf{M}_i \times \mathbf{B}_{\text{eff}}^i)], \quad (3)$$

using the Heun numerical scheme with projection to the unit sphere [23]. Here $\mathbf{B}_{\text{eff}}^i = -\frac{1}{\mu_M} \partial \mathcal{H} / \partial \mathbf{M}_i$ is the effective magnetic field (μ_M is the magnitude of localized magnetic moments); g is the gyromagnetic ratio; and the intrinsic Gilbert damping parameter λ arises due to the well-established mechanism [32, 33] combining spin-orbit coupling and electron-phonon interactions.

The conduction electron subsystem is modeled by a quantum Hamiltonian

$$\hat{H} = -\gamma \sum_{\langle ij \rangle} \hat{c}_i^\dagger \hat{c}_i - J_{sd} \sum_i \hat{c}_i^\dagger \boldsymbol{\sigma} \cdot \mathbf{M}_i(t) \hat{c}_i, \quad (4)$$

where the first term is a 1D tight-binding (TB) model and the second term is the s - d exchange coupling between conduction electrons and localized magnetic moments. Here $\hat{c}_i^\dagger = (\hat{c}_{i\uparrow}^\dagger, \hat{c}_{i\downarrow}^\dagger)$ is a row vector containing operators $\hat{c}_{i\sigma}^\dagger$ which create an electron of spin $\sigma = \uparrow, \downarrow$ at the site i , and \hat{c}_i is a column vector that contains the corresponding annihilation operators. The magnetic nanowire in the setup in Fig. 1 consists of 45 sites and it is attached to semi-infinite NM leads modeled by the first term alone in Eq. (4). The nearest-neighbor hopping is $\gamma = 1$ eV and the Fermi energy is set at $E_F = 0$ eV (or $E_F - E_b = 2.0$ eV if measured from the band bottom, $E_b = -2.0\gamma$, of the NM leads). The quantum dynamics of the electrons is described by solving a matrix integro-differential equation [41, 42]

$$i\hbar \frac{d\rho_{\text{neq}}}{dt} = [\mathbf{H}, \rho_{\text{neq}}] + i \sum_{p=L,R} [\boldsymbol{\Pi}_p(t) + \boldsymbol{\Pi}_p^\dagger(t)]. \quad (5)$$

This can be viewed as the exact master equation for an open finite-size quantum system, described by \hat{H} and its matrix representation \mathbf{H} , that is attached (via semi-infinite NM leads) to macroscopic reservoirs. The matrices ρ_{neq} and $\boldsymbol{\Pi}_p$ are expressed in terms of TD-NEGFs [38] and/or integrals over them, as elaborated in Refs. [41, 42]. The $\boldsymbol{\Pi}_p$ matrices yield the charge, $I_p(t) = \frac{e}{\hbar} \text{Tr} [\boldsymbol{\Pi}_p(t)]$, and the spin, $I_p^{S\alpha}(t) = \frac{e}{\hbar} \text{Tr} [\hat{\sigma}_\alpha \boldsymbol{\Pi}_p(t)]$, currents flowing into the NM lead $p = L, R$.

In the TDNEGF+LLG framework [26, 30] we self-consistently combine quantum Eqs. (2) and (5) with classical Eq. (3) by first solving for $\langle \hat{S} \rangle_i^{\text{neq}}(t)$ using Eq.(2), which is then fed into Eq. (3) to propagate localized mag-

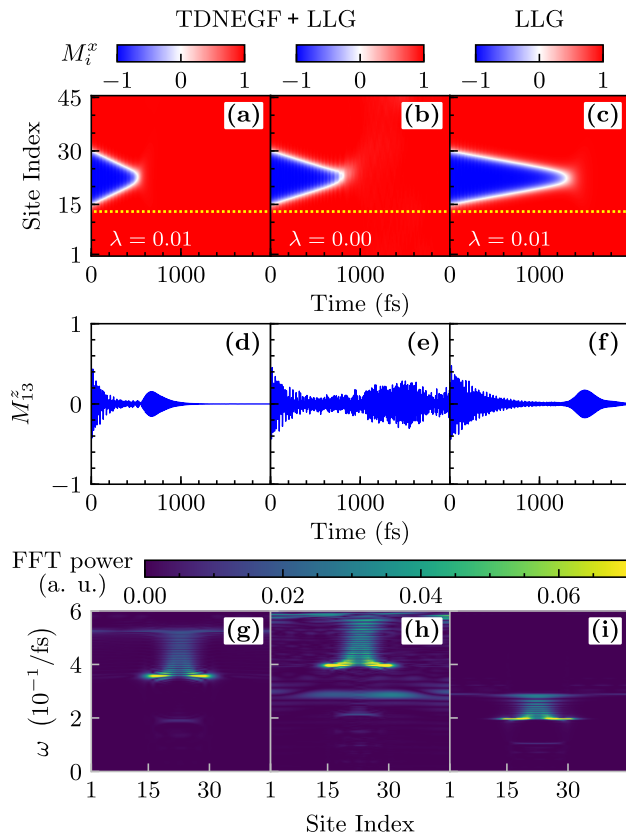


FIG. 4. (a)–(c) Spatio-temporal profiles of the x -component of localized magnetic moments $M_i^x(t)$. (d)–(f) Time dependence of the z -component $M_{13}^z(t)$ of a localized magnetic moment at the site $i = 13$ [marked by a horizontal dashed line in panels (a)–(c)]. (g)–(i) Frequency power spectra [20] obtained from FFT of $M_{13}^z(t)$ time-dependence over 0–2 ps time interval. The first and second column of panels is obtained from TDNEGFB+LLG simulations with the intrinsic Gilbert damping $\lambda = 0.01$ or $\lambda \equiv 0$, respectively. The third column of the panels is obtained from LLG equation, as in purely classical micromagnetics simulations of DW annihilation [8–10, 18], with the intrinsic Gilbert damping $\lambda = 0.01$.

netic moments $\mathbf{M}_i(t)$ in the next time step. The time step $\delta t = 0.1$ fs is used for numerical stability, and recently developed TDNEGFB algorithms scaling linearly [39, 42] in the number of time steps are employed. These updated $\mathbf{M}_i(t)$ classical vectors are fed back into the quantum Hamiltonian of the conduction electron subsystem in Eq. (4). Thus obtained time-dependences of $\mathbf{M}_i(t)$, $\langle \hat{\mathbf{S}} \rangle_i^{\text{neq}}(t)$, $I_p(t)$ and $I_p^{S_\alpha}(t)$ are numerically exact.

Figure 2(a) shows TDNEGFB+LLG computed snapshots of the localized magnetic moments $\mathbf{M}_i(t)$ for a subset of sites $i = 12$ –33 in the course of DW collision and annihilation at selected times. The corresponding complete spatio-temporal profiles are animated as a movie provided in the Supplemental Material (SM) [43]. In addition, Fig. 2(b)–(d) shows spatio-temporal profiles of $\text{STT} \propto \langle \hat{\mathbf{S}} \rangle_i^{\text{neq}}(t) \times \mathbf{M}_i(t)$ at all sites $i = 1$ –45. Such

STT generated by TDNEGFB calculations, which is absent in purely classical micromagnetics simulations, is due to moving electrons comprising spin currents [Fig. 3] pumped by time-dependent fields $\mathbf{M}_i(t)$ entering into the second term of the quantum Hamiltonian of electronic subsystem in Eq. (4). The noncollinearity of $\langle \hat{\mathbf{S}} \rangle_i^{\text{neq}}(t)$ and $\mathbf{M}_i(t)$ required for nonzero STT originates from the fact that the motion of the classical localized magnetic moments affects the conduction electrons in a *retarded way*—it takes a finite time until the local conduction electron spin reacts to the dynamics of $\mathbf{M}_i(t)$, no matter how slow that dynamics is [30]. Thus, $\langle \hat{\mathbf{S}} \rangle_i^{\text{neq}}(t)$ is always somewhat behind the “adiabatic direction” set by $\mathbf{M}_i(t)$ [31].

The snapshot at $t = 520$ fs in Fig. 2(a) shows two DWs vanishing since $M_i^x > 0$ at all sites i . The quantum transport signature of this process is the reduction in the magnitude of pumped electronic spin currents [Fig. 3(a)–(c)]. In fact, $I_R^{S_x}(t) \rightarrow 0$ component becomes zero [Fig. 3(a)] at $t = 645$ fs at which localized magnetic moments in Fig. 2(a) turn nearly parallel to the x -axis while precessing around it. Such oscillations excited within the annihilation region in the middle of the magnetic nanowire propagate toward the NM leads in the form of a traveling wave, see Fig. 2(e) and the movie in the SM [43], as the signature of SW burst. The frequency power spectrum [red curve in Fig. 3(d)] obtained from fast Fourier transform (FFT) of $I_R^{S_z}(t)$, for times prior to completed annihilation and SW burst at $t = 645$ fs, reveal highly unusual *spin pumping over a broadband frequency range*. This can be compared to the usual spin current pumping [25] whose power spectrum is just a peak around a single frequency [44], as also obtained [brown curve in Fig. 3(d)] by FFT of $I_R^{S_z}(t)$ at post-annihilation times $t > 645$ fs.

The total spin current in Fig. 3(a)–(c) has contributions from both electrons moved by time-dependent $\mathbf{M}_i(t)$ and SW hitting the magnetic-nanowire/nonmagnetic-NM-lead interface. That is, at this interface, SW spin current is stopped and “transmuted” [45] into an electronic spin current flowing into the NM lead. The “transmutation” is often employed experimentally for direct electrical detection of SWs, where an electronic spin current on the NM side is converted into a voltage signal via the inverse spin Hall effect [18, 46]. Within the TDNEGFB+LLG picture, SW reaching the last localized magnetic moments of the magnetic nanowire, at the sites $i = 1$ or $i = 45$ in our setup, initiates their dynamics whose coupling to conduction electrons in the neighboring left and right NM leads, respectively, leads to pumping [25, 28] of the electronic spin current into the NM leads.

In order to quantify electronic spin current due “transmutation” from SW burst, which we denote by $I_p^{S_\alpha, \text{SW}}$, we first record all trajectories $\mathbf{M}_i(t)$ from full TDNEGFB+LLG calculations, and then feed them into pure

TDNEGF calculations using the Hamiltonian in Eq. (4) but with only $\mathbf{M}_1(t)$ and $\mathbf{M}_{45}(t)$ being coupled to conduction electrons. This procedure is justified by Fig. 3(e)–(g) where $I_R^{S_\alpha, \text{SW}}$ is either zero or very small until the SW burst is generated, while the spin current [Fig. 3(a)–(c)] carrying electrons from the bulk of the nanowire into the NM leads remains large within the same time frame. Comparison [Fig. 3(e)–(g)] of SW contribution with bulk electron contribution to the pumped spin current at post-annihilation times $t > 645$ fs shows that they are of a similar magnitude. This is in contrast to classical micromagnetics interpretation of recent DW annihilation experiments [18] where the detected electronic spin current in the NM leads was attributed solely to SWs.

The STT [Fig. 2(b)–(d)] due to pumped spin current can effectively act as an additional Gilbert damping [30, 31] in the LLG equation, which can be an order of magnitude larger [26] than the intrinsic Gilbert damping [32, 33]. It can also exhibit time-retardation described by a memory kernel [30]. Therefore, we compare in Fig. 4 TDNEGF+LLG calculated trajectories $\mathbf{M}_i(t)$ using nonzero [Fig. 4(a),(d)] vs. zero [Fig. 4(b),(e)] intrinsic Gilbert damping; as well as those results vs. purely LLG calculated trajectories [Fig. 4(c),(f)]. The corresponding frequency power spectra [20] [Fig. 4(g)–(i)] are obtained from FFT of $M_i^z(t)$ time-dependence. These comparisons reveal that additional *nonlocal-in-time* damping generated by time-retardation effects [31, 35, 36] in the full TDNEGF+LLG scheme [30] *cannot* be mimicked by simply adjusting the magnitude of standard *local-in-time* Gilbert damping term $\lambda \mathbf{M}_i(t) \times d\mathbf{M}_i(t)/dt$ [note that Eq. (3) uses equivalent Landau-Lifshitz form of this term [23]]. We note that memory kernel can be explicitly extracted [30] in terms of TDNEGF quantities only in the case of small J_{sd} and weak a coupling to macroscopic reservoirs. Physically, it describes how nonequilibrium electrons mediate interaction of $\mathbf{M}_i(t)$ with the same localized magnetic moment at an earlier time $t' < t$.

Finally, we note that broadband pumped spin current from Fig. 3(d) can be converted into rapidly changing transient charge current via the inverse spin Hall effect [47]. Such charge current will, in turn, emit electromagnetic radiation that can be brought into THz range, thereby offering broadband THz emission from a spintronic device.

M. D. P. and P. P. were supported by ARO MURI Award No. W911NF-14-0247. B. K. N. was supported by NSF Grant No. ECCS 1922689. This work used the Extreme Science and Engineering Discovery Environment (XSEDE), which is supported by NSF grant No. ACI-1548562.

* bnikolic@udel.edu

- [1] G. Tatara, H. Kohno, and J. Shibata, Microscopic approach to current-driven domain wall dynamics, *Phys. Rep.* **468**, 213 (2008).
- [2] K.-J. Kim, Y. Yoshimura, and T. Ono, Current-driven magnetic domain wall motion and its real-time detection, *Jap. J. Appl. Phys.*, **56** 0802A4 (2017).
- [3] S. Parkin and S.-H. Yang, Memory on the racetrack, *Nat. Nanotech.* **10** 195 (2015).
- [4] D. A. Allwood, G. Xiong, M. D. Cooke, C. C. Faulkner, D. Atkinson, N. Vernier, and R. P. Cowburn, Submicrometer ferromagnetic not gate and shift register, *Science* **296**, 2003 (2002).
- [5] J. Grollier, D. Querlioz, and M. D. Stiles, Spintronic nanodevices for bioinspired computing, *Proc. IEEE* **104**, 2024 (2016).
- [6] L. Thomas, M. Hayashi, R. Moriya, C. Rettner, and S. Parkin, Topological repulsion between domain walls in magnetic nanowires leading to the formation of bound states, *Nat. Commun.* **3**, 810 (2012).
- [7] H.-B. Braun, Topological effects in nanomagnetism: From superparamagnetism to chiral quantum solitons, *Adv. Phys.* **61**, 1 (2012).
- [8] A. Kunz, Field induced domain wall collisions in thin magnetic nanowires, *Appl. Phys. Lett.* **94**, 132502 (2009).
- [9] A. Kunz and E. W. Rentsch, Simulations of field driven domain wall interactions in ferromagnetic nanowires, *IEEE Trans. Magn.* **46**, 1556 (2010).
- [10] A. Ghosh, K. S. Huang, and O. Tchernyshyov, Annihilation of domain walls in a ferromagnetic wire, *Phys. Rev. B* **95**, 180408 (2017).
- [11] S. K. Kim, S. Takei, and Y. Tserkovnyak, Topological spin transport by Brownian diffusion of domain walls, *Phys. Rev. B* **92**, 220409 (2015).
- [12] D. I. Bradley, S. N. Fisher, A. M. Gunault, R. P. Haley, J. Kopu, H. Martin, G. R. Pickett, J. E. Roberts, and V. Tsepelin, Relic topological defects from brane annihilation simulated in superfluid ^3He , *Nature Phys.* **4**, 46 (2008).
- [13] N. Manton and P. Sutcliffe, *Topological solitons* (Cambridge University Press, Cambridge, 2004).
- [14] G. Dvali and A. Vilenkin, Solitonic D-branes and brane annihilation, *Phys. Rev. D* **67**, 046002 (2003).
- [15] H. Takeuchi, K. Kasamatsu, M. Tsubota, and M. Nitta, Tachyon condensation due to domain-wall annihilation in Bose-Einstein condensates, *Phys. Rev. Lett.* **109**, 245301 (2012).
- [16] M. Nitta, K. Kasamatsu, M. Tsubota, and H. Takeuchi, Creating vortons and three-dimensional skyrmions from domain-wall annihilation with stretched vortices in Bose-Einstein condensates, *Phys. Rev. A* **85**, 053639 (2012).
- [17] Y. Shen and I. Dierking, Annihilation dynamics of topological defects induced by microparticles in nematic liquid crystals, *Soft Matter* **10**.1039/C9SM01710K (2019).
- [18] S. Woo, T. Delaney, and G. S. D. Beach, Magnetic domain wall depinning assisted by spin wave bursts, *Nat. Phys.* **13**, 448 (2017).
- [19] A. V. Chumak, V. I. Vasyuchka, A. A. Serga, and B. Hillebrands, Magnon spintronics, *Nat. Phys.* **11**, 453 (2015).
- [20] S.-K. Kim, Micromagnetic computer simulations of spin

waves in nanometre-scale patterned magnetic elements, *J. Phys. D: Appl. Phys.* **43**, 264004 (2010).

[21] A. Navabi *et al.*, Efficient excitation of high-frequency exchange-dominated spin waves in periodic ferromagnetic structures, *Phys. Rev. Applied* **7**, 034027 (2017).

[22] C. Liu *et al.*, Long-distance propagation of short-wavelength spin waves, *Nat. Commun.* **9**, 738 (2018).

[23] R. F. L. Evans, W. J. Fan, P. Chureemart, T. A. Ostler, M. O. A. Ellis, and R. W. Chantrell, Atomistic spin model simulations of magnetic nanomaterials, *J. Phys.: Condens. Matter* **26**, 103202 (2014).

[24] P. Mondal, U. Bajpai, M. D. Petrović, P. Plecháč, and B. K. Nikolić, Quantum spin transfer torque induced nonclassical magnetization dynamics and electromagnetization entanglement, *Phys. Rev. B* **99**, 094431 (2019).

[25] Y. Tserkovnyak, A. Brataas, G. E. W. Bauer, and B. I. Halperin, Nonlocal magnetization dynamics in ferromagnetic heterostructures, *Rev. Mod. Phys.* **77**, 1375 (2005).

[26] M. D. Petrović, B. S. Popescu, U. Bajpai, P. Plecháč, and B. K. Nikolić, Spin and charge pumping by a steady or pulse-current-driven magnetic domain wall: A self-consistent multiscale time-dependent quantum-classical hybrid approach, *Phys. Rev. Applied* **10**, 054038 (2018).

[27] L. E. F. Foa Torres, Mono-parametric quantum charge pumping: Interplay between spatial interference and photon-assisted tunneling, *Phys. Rev. B* **72**, 245339 (2005).

[28] S.-H. Chen, C.-R. Chang, J. Q. Xiao, and B. K. Nikolić, Spin and charge pumping in magnetic tunnel junctions with precessing magnetization: A nonequilibrium Green function approach, *Phys. Rev. B* **79**, 054424 (2009).

[29] U. Bajpai, B. S. Popescu, P. Plecháč, B. K. Nikolić, L. E. F. Foa Torres, H. Ishizuka, and N. Nagaosa, Spatio-temporal dynamics of shift current quantum pumping by femtosecond light pulse *J. Phys.: Mater.* **2**, 025004 (2019).

[30] U. Bajpai and B. K. Nikolić, Time-retarded damping and magnetic inertia in the Landau-Lifshitz-Gilbert equation self-consistently coupled to electronic time-dependent nonequilibrium Green functions, *Phys. Rev. B* **99**, 134409 (2019).

[31] M. Sayad and M. Potthoff, Spin dynamics and relaxation in the classical-spin Kondo-impurity model beyond the Landau-Lifshitz-Gilbert equation, *New J. Phys.* **17**, 113058 (2015).

[32] V. Kamberský, Spin-orbital Gilbert damping in common magnetic metals, *Phys. Rev. B* **76**, 134416 (2007).

[33] K. Gilmore, Y. U. Idzerda, and M. D. Stiles, Identification of the dominant precession-damping mechanism in Fe, Co, and Ni by first-principles calculations, *Phys. Rev. Lett.* **99**, 027204 (2007).

[34] P. Chureemart, I. D'Amico, and R. W. Chantrell, Model of spin accumulation and spin torque in spatially varying magnetisation structures: Limitations of the micromagnetic approach, *J. Phys.: Condens. Matter* **27**, 146004 (2015).

[35] T. Bose and S. Trimper, Retardation effects in the Landau-Lifshitz-Gilbert equation, *Phys. Rev. B* **83**, 134434 (2011).

[36] D. Thonig, J. Henk, and O. Eriksson, Gilbert-like damping caused by time retardation in atomistic magnetization dynamics, *Phys. Rev. B* **92**, 104403 (2015).

[37] E. V. Boström and C. Verdozzi, Steering magnetic skyrmions with currents: A nonequilibrium Greens functions approach, *Phys. Stat. Solidi B* **256**, 1800590 (2019).

[38] G. Stefanucci and R. van Leeuwen, *Nonequilibrium Many-Body Theory of Quantum Systems: A Modern Introduction* (Cambridge University Press, Cambridge, 2013).

[39] B. Gaury, J. Weston, M. Santin, M. Houzet, C. Groth, and X. Waintal, Numerical simulations of time-resolved quantum electronics, *Phys. Rep.* **534**, 1 (2014).

[40] F. Mahfouzi and B. K. Nikolić, How to construct the proper gauge-invariant density matrix in steady-state nonequilibrium: Applications to spin-transfer and spin-orbit torques, *SPIN* **3**, 1330002 (2013).

[41] A. Croy and U. Saalmann, Propagation scheme for nonequilibrium dynamics of electron transport in nanoscale devices, *Phys. Rev. B* **80**, 245311 (2009).

[42] B. S. Popescu and A. Croy, Efficient auxiliary-mode approach for time-dependent nanoelectronics, *New J. Phys.* **18**, 093044 (2016).

[43] See Supplemental Material at <https://wiki.physics.udel.edu/qttg/Publications> for a movie, accompanying Figs. 2 and 4, which animates time evolution of localized magnetic moments $\mathbf{M}_i(t)$ in the course of DW collision and annihilation, as obtained from TDNEGF+LLG simulations.

[44] L. Bocklage, Coherent THz transient spin currents by spin pumping, *Phys. Rev. Lett.* **118**, 257202 (2017).

[45] G. E. Bauer and Y. Tserkovnyak, Viewpoint: spin-magnon transmutation, *Physics* **4**, 40 (2011).

[46] A. V. Chumak, A. A. Serga, M. B. Jungfleisch, R. Neb, D. A. Bozhko, V. S. Tiberkevich, and B. Hillebrands, Direct detection of magnon spin transport by the inverse spin Hall effect, *Appl. Phys. Lett.* **100**, 082405 (2012).

[47] M. Chen, Y. Wu, Y. Liu, K. Lee, X. Qiu, P. He, J. Yu, and H. Yang, Current-enhanced broadband THz emission from spintronic devices, *Adv. Optical Mater.* **7**, 1801608 (2019).